Model and Observations of Dielectric Charge in Thermally Oxidized Silicon Resonators

Gaurav Bahl, Renata Melamud, Bongsang Kim, Saurabh A. Chandorkar, James C. Salvia, Matthew A. Hopcroft, *Member, IEEE*, David Elata, *Member, IEEE*, Robert G. Hennessy, Rob N. Candler, Roger T. Howe, *Fellow, IEEE*, and Thomas W. Kenny

***Abstract*—This paper investigates the effects of dielectric charge on resonant frequency in thermally oxidized silicon resonators hermetically encapsulated using "epi-seal." SiO_2 coatings are effective for passive temperature compensation of resonators but make the devices more susceptible to charging-related issues. We present a theoretical model for the electromechanical effects of charge trapped in the dielectrics within the transduction gap of a resonator. Observations of resonance frequency against varying resonator bias voltage are fitted to this model in order to obtain estimates for the magnitude of the trapped oxide charge. Statistics collected from wet- and dry-oxidized devices show that lower fixed oxide charge can be expected upon dry oxidation. In addition, observations of time-varying resonator frequency indicate the presence of mobile oxide charge in a series of voltage biasing and temperature experiments. [2009-0088]**

***Index Terms*—Charging, dielectrics, frequency drift, reliability, resonators, silicon dioxide.**

I. Introduction

SILICON micromechanical resonators have recently come into view as competitors to quartz technology for frequency reference applications [2]. Several researchers have investigated techniques for the active and passive compensation of silicon resonators [3]–[7]. In particular, a promising temperature compensation technique exploiting the positive temperature coefficient of an elastic modulus of silicon dioxide [8] has been demonstrated by several researchers for microelectromechanical systems (MEMS) [9]–[12] and for surface acoustic wave devices [13], [14]. In the case of the tuning fork resonators designed and built in [9], it has been seen that the thermal silicon dioxide coating these resonators is susceptible to charging issues [1]. Dielectric charging is of broad interest to the MEMS community since dielectrics like silicon nitride and silicon dioxide are often used as electrical and mechanical materials. The typical solution to circumvent the charging problem is to completely avoid the use of dielectrics where possible. For frequency references, however, active compensation systems require more power and complexity, and thus, passive compensation techniques (such as oxide coatings) become essential to support them.

Dielectric charging in contacting structures such as RF capacitive switches has been studied extensively [15]–[19]. In these structures, capacitance measurements are used to infer the charge through partial deflection [18] or complete pull-in measurements [19]. In stiff noncontacting structures such as resonators, accelerometers, and gyroscopes, charge buildup can also affect the long-term stability and reliability of transducers. Pull-in measurements are often impractical for such structures and do not emulate standard operating conditions that these devices see. In such cases, the use of resonant frequency measurements can complement or replace pull-in measurements as a noncontact method to study the evolution of charge in dielectrics particularly under low-field conditions (less than 10^6 V/cm).

In this study, oxide-coated composite-beam silicon resonators designed previously by Melamud *et al.* [9] were used as a testbed for dielectric layers within the transduction gap of a resonator. An electrostatics-based model is presented for the electromechanical effects of charge trapped in this dielectric. Experimental data show agreement with the model, indicating the presence of a built-in voltage in the devices. The built-in voltage can be mapped back to an equivalent dielectric-trapped charge by fitting to the model. In this manner, charge estimations were obtained from multiple devices, indicating that dry oxidation, on average, yields a lower amount of fixed dielectric charge. Evidence for mobile charge in a small proportion of wet-oxidized devices is also presented through a series of experiments. In all these tests, lithographically identical silicon-only resonators with no native oxide are used to confirm the stability of the applied bias voltage and environmental temperature since they represent the zero-dielectric and zero-charge case.

Manuscript received April 7, 2009; revised August 17, 2009. First published December 4, 2009; current version published February 3, 2010. This work was supported in part by the Defense Advanced Research Projects Agency (DARPA) under Grant HR0011-06-0049 (Dr. D. L. Polla, Program Manager); by Bosch; by Epson; by HP; by Agilent; by Boeing; by Qualcomm; by DARPA Harsh Environment Robust Micromechanical Technology under Grant ONR N66001-03-1-8942; by the National Nanofabrication Users Network facilities, funded by the National Science Foundation under Award ECS-9731294; and by the National Science Foundation Instrumentation for Materials Research Program under Grant DMR 9504099. Subject Editor C. Hierold.

G. Bahl, J. C. Salvia, R. G. Hennessy, and R. T. Howe are with the Department of Electrical Engineering, Stanford University, Stanford, CA 94305-9505 USA (e-mail: bahlg@stanford.edu).

R. Melamud is with SiTime Corporation, Sunnyvale, CA 94085 USA.

B. Kim and M. A. Hopcroft are with the Berkeley Sensor and Actuator Center, University of California, Berkeley, CA 94720-1774 USA.

S. A. Chandorkar and T. W. Kenny are with the Mechanical Engineering Department, Stanford University, Stanford, CA 94305-3030 USA.

D. Elata is with the Mechanical Engineering Micro-Systems Laboratory, Faculty of Mechanical Engineering, Technion—Israel Institute of Technology, Haifa 32000, Israel.

R. N. Candler is with the Sensors and Technology Laboratory, University of California, Los Angeles, CA 90095 USA.

Color versions of one or more of the figures in this paper are available online at http://ieeexplore.ieee.org.

Digital Object Identifier 10.1109/JMEMS.2009.2036274

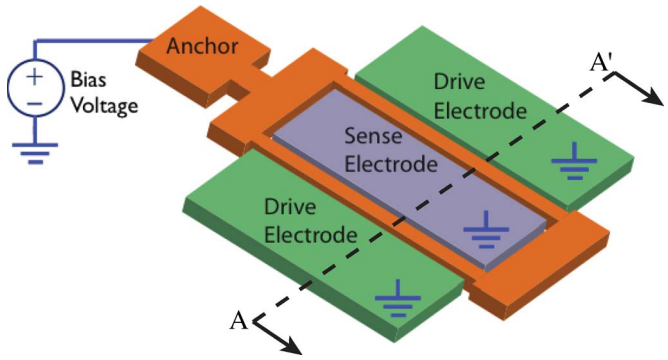

Fig. 1. Single-anchor DETF resonators used in this paper. The cross section A–A' is shown in Fig. 2.

II. Resonator Design and Fabrication

A. Design

Single-anchored double-ended tuning fork (DETF) resonators (Fig. 1) were built to operate in flexural mode between 400 kHz and 2 MHz depending on the specific beam dimensions. The single-anchor design prevents substrate, package, and oxide stress from coupling to the beams and affecting the resonance frequency. Actuation of the symmetric mode is enforced by symmetrically placed drive electrodes on the sides of the two beams. The central electrode is used for sensing the motion of the resonator through capacitive coupling. The electrical configuration of the resonators is discussed later in Section IV-A.

B. Fabrication and Encapsulation Environment

The resonators are fabricated in single crystal silicon using silicon-on-insulator wafers with a 20-μm device layer. The resonators are encapsulated using the "epi-seal" encapsulation technology that has been discussed previously by Candler *et al.* [20]. In this process, the wafer-scale sealing is performed in an epitaxial deposition chamber at 1100 °C in the presence of hydrogen and nitrogen gas and the silicon precursor dichlorosilane. This high-temperature step vaporizes native silicon dioxide, as well as any organics that are present in the resonator cavity. Such temperature-based removal of native oxide has been studied previously [21], [22]. Furthermore, the absence of oxygen and the presence of large amounts of hydrogen and nitrogen gas prevent any oxide from forming on the devices after sealing. As a result, this encapsulation technique gives us a test environment with zero native oxide.

The estimated pressure inside the encapsulation is about 1 Pa [23] and, for our devices, yields quality factors of about 10 000–30 000. The devices have been shown to be very stable [23], [24] since they are protected against many of the common environmental issues such as dust, corrosive and oxidizing agents, and moisture. The primary stimulus that can physically affect the resonators at this point is the temperature, and that too can be controlled through the use of a temperature-controlled chamber.

C. Dielectric Coating

The fabrication of oxidized versions of these devices has been discussed by Melamud *et al.*[25]. Since thermal oxidation is a well-understood reaction-rate-limited process step, we can assume that oxidation, if carefully performed, creates a fairly uniform layer of oxide on all exposed silicon surfaces within the cavity. In addition, a variety of oxide growth conditions can be experimented with, and a variety of postoxidation treatments can be tested. For the purposes of this study, we restricted the oxidation to dry (oxygen ambient) and wet (steam grown) thermal oxides.

The oxidation is performed in furnaces maintaining CMOS-grade cleanliness. Wet oxidation is performed at 1100 °C in a steam ambient and takes 30 min–1 h for thick oxides. The furnace automatically performs a dry-oxidation step before and after the wet-oxidation step, resulting in a dry–wet–dry oxide stack. Dry oxidation is performed at 1100 °C in a dry oxygen ambient for 5–9 h depending on the required oxide thickness. Since our thermal oxides are significantly thicker than a native oxide layer, they can survive the high-temperature sealing step. The as-designed presence of the thermal oxide in the finished devices has been confirmed through sectioning test wafers at the end of the process [25] and with the mapping of temperature–frequency characteristics [9]. In this paper, dry oxide of 0.35 μm thickness and wet oxide of 0.42 μm thickness are studied.

III. Modeling Charge Effects

Recent parallel work by Kalicinski *et al.* [26] models the effects of charge on resonator frequency. The presence of a thin native oxide is assumed on the silicon resonators, and the charge is modeled through an empirical correction to the dc bias voltage that they define as $V_{\rm shift}$. The effect of this parasitic voltage is mapped to the frequency through the equation $f_s \approx f_o\sqrt{1 - A(V_{\rm dc}/V_{\rm PI})^2}$ that demonstrates a quadratic dependence on the dc bias voltage $(V_{\rm dc})$. This equation is derived from the work of Tilmans and Legtenberg [27] and is valid when the axial load on a resonant beam is zero, which is true for single-anchored devices. However, the pull-in voltage $(V_{\rm PI})$ description becomes ambiguous in cases with charged dielectrics since the observable pull-in voltage is different (and often variable) for positive and negative biasing [15], [28], [29]. The model presented in [26] assumes that the polarization of the dielectric is negligible. In general, for finite-thickness dielectrics, the voltage $V_{\rm shift}$ described in the figures in [26] as the voltage across the dielectric will depend on the dc bias voltage applied to the device.

The following sections present an analysis of the effects of charge and finite-thickness dielectrics based on the energy method without the need for a thin oxide simplification. We employ a different approach, where charge is associated to the change of frequency by affecting a softening modification to the effective spring constant of the resonator through $f_o' \approx f_o(1 - k_e/2k_m)$. This method has been previously described by several studies [30]–[32] and is more general (for an arbitrary axial load, for instance) as long as the mechanical spring constant of the resonator k_m and its resonance frequency f_o can be modeled

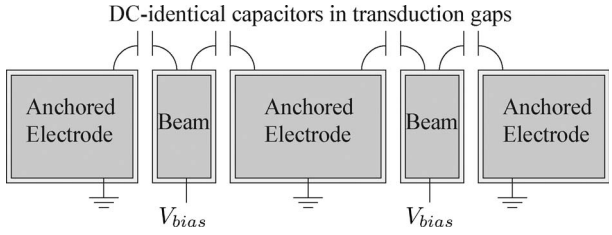

Fig. 2. Device cross section A–A' from Fig. 1 indicating four identical capacitors in dc representation. The electrostatic pull force on each capacitor is identical and is analyzed using the single-capacitor model in Fig. 3.

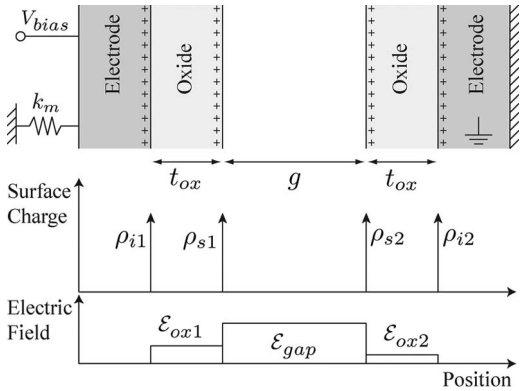

Fig. 3. Single-capacitor model for the analysis of the electromechanical effects from the charge and voltage (leading in from Fig. 2). Only the surface charge sheets at the oxide–air interface are considered. All charge is assumed to be a positive delta function for sign convention and representation purposes. Damping and quality factor are not part of this model.

or determined. The electrostatic spring modification k_e is dependent on the dc bias voltage and the geometry. Our model mathematically explains how dielectric charge changes the effective dc bias voltage applied to the device (and thus, k_e) by mapping its effects into an indirectly observable built-in voltage ($V_{\rm bi}$ in this paper, denoted $V_{\rm shift}$ in [26]). This enables us, to some extent, to extract the amount of charge that is present in the system through frequency observations.

A. Physical Model

The resonator beams form four capacitors with the three electrodes adjacent to them, as shown in Fig. 2. It is reasonable to treat these as parallel plate capacitors since the device layer thickness (20 μm) and the beam length ($\sim$200 μm) are much larger than the lithographically defined actuation gap of 1.5 μm.

Electrically, both stimulus and sense electrodes are held at a dc ground potential, although they do carry a small ac resonance signal. The mechanical structure is biased at a constant dc potential $V_{\rm bias}$. As a result, the dc electromechanical representation of all four of these capacitors is identical. Thus, the electrostatic pull force on each capacitor is also identical and can be modeled with the same common variables with a single-capacitor mass–spring lumped model, as shown in Fig. 3. This is a simplifying assumption for this analysis since the charge state of each individual capacitor is unknown.

B. Electromechanics From Energy Method

The following derivation goes through an analysis of the effects of charge and voltage on the electromechanical properties of a resonator that is operating in the linear regime. Although the following symbolic analysis is presented for the special case of a system where there are two symmetric dielectrics, the methodology used in this derivation is broadly applicable, and the end result can be rederived for other electrostatic actuators (such as with one dielectric, unequal dielectrics, or multiple dielectrics). It is assumed that the charge is only present at the oxide–air interface of the dielectrics. The bulk-charge case is considered in Section III-C as an extension of the result obtained for surface charge. Since the nature of the charge in the dielectrics may be unknown and the bias voltage can vary, we cannot *a priori* assume the polarity of the surface charges in any part of the system. Therefore, the charge is assumed to be positive in all cases. Dealing with a negative charge simply involves a sign reversal, and the solutions will yield appropriate signs when negative charge is present.

The proposed solution method is to determine the total energy in the system $U_{\rm sys}$. This includes the energy stored in the field within the capacitors $U_{\rm fields}$ and the contribution of the bias voltage source $U_V = U_V^0 + \Delta U_V$, where U_V^0 is the unknown but constant energy associated with the voltage source before the x displacement "probe" is applied. The negative gradient of this energy with respect to the displacement of the mobile structure is the attractive force acting on the capacitor plates. Then, linearizing the force equation and accounting for both transduction capacitors around the resonator beam, one can obtain an effective spring constant for the beam. The effects of charge appear as a modification to the spring-softening effect that is usually caused due to bias voltage alone.

The model of one capacitor with variable definitions is shown in Fig. 3. Here, ρ_{s1} and ρ_{s2} are uniform surface charge sheets assumed to be present at the oxide–air interface of each dielectric layer. The oxide thickness $t_{\rm ox}$ is taken to be identical on both electrodes. The portion of the transduction gap that is only air (or vacuum) has a spacing g. For this analysis, the electrodes are assumed to be highly doped and are consequently assumed metallic in behavior. Accumulation and depletion effects of silicon are not considered. The electric fields within the oxides and air gap are indicated as $\mathcal{E}_{\rm ox1}$, $\mathcal{E}_{\rm ox2}$, and $\mathcal{E}_{\rm gap}$, respectively. In addition, ρ_{i1} and ρ_{i2} are the surface charge densities induced on the electrode surfaces due to the applied voltages and electric fields in the system. These charge sheets are provided by the voltage source.

Using Gauss's law and the assumed metallic nature of the electrodes, the following expression must hold true for any biasing condition:

$$\rho_{s1} + \rho_{s2} + \rho_{i1} + \rho_{i2} = 0. \tag{1}$$

Through repeated application of Gauss's law, we then arrive at the expressions defining the electric fields within the dielectrics and the vacuum/air gap

$$\mathcal{E}_{\rm ox1} = \frac{\rho_{i1}}{\epsilon_{\rm ox}} \tag{2}$$

$$\mathcal{E}_{\rm gap} = \frac{\rho_{i1} + \rho_{s1}}{\epsilon_o} \tag{3}$$

$$\mathcal{E}_{\rm ox2} = \frac{\rho_{i1} + \rho_{s1} + \rho_{s2}}{\epsilon_{\rm ox}}. \tag{4}$$

In addition, the potential drop between the two plates as obtained through the electric fields must equal the bias potential applied externally

$$\mathcal{E}_{\rm ox1}t_{\rm ox} + \mathcal{E}_{\rm gap}(g-x) + \mathcal{E}_{\rm ox2}t_{\rm ox} = V_{\rm bias} \tag{5}$$

where x is a minute displacement of the mobile electrode, i.e., resonant beam. Since there are five unknowns ($\mathcal{E}_{\rm ox1}$, $\mathcal{E}_{\rm gap}$, $\mathcal{E}_{\rm ox2}$, ρ_{i1}, and ρ_{i2}) and five equations, we can solve for all fields and induced charges. Specifically, we need ρ_{i1} and ρ_{i2} to determine the energy lost by the voltage source

$$\rho_{i1} = \frac{(V_{\rm bias}\epsilon_o\epsilon_{\rm ox} - (g-x)\epsilon_{\rm ox}\rho_{s1} - t_{\rm ox}\epsilon_o(\rho_{s1}+\rho_{s2}))}{2t_{\rm ox}\epsilon_o + (g-x)\epsilon_{\rm ox}} \tag{6}$$

$$\rho_{i2} = \frac{(-V_{\rm bias}\epsilon_o\epsilon_{\rm ox} - (g-x)\epsilon_{\rm ox}\rho_{s2} - t_{\rm ox}\epsilon_o(\rho_{s1}+\rho_{s2}))}{2t_{\rm ox}\epsilon_o + (g-x)\epsilon_{\rm ox}}. \tag{7}$$

The work done by the voltage source in order to move these induced charges onto the electrodes is

$$\Delta U_V = -V_{\rm bias}\left(\frac{A\rho_{i1} - A\rho_{i2}}{2}\right) \tag{8}$$

where A is the electrode area required to convert from a surface charge density to the net charge on the electrodes. When the charge in the dielectrics is zero, this reduces to

$$\begin{aligned}\Delta U_V|_{\rm no\,oxide\,charge} &= -\frac{AV_{\rm bias}}{2}\left(\frac{2V_{\rm bias}\epsilon_o\epsilon_{\rm ox}}{2t_{\rm ox}\epsilon_o + (g-x)\epsilon_{\rm ox}}\right) \\ &= -\frac{A\epsilon_o\epsilon_{\rm ox}}{2t_{\rm ox}\epsilon_o + g\epsilon_{\rm ox}}V_{\rm bias}^2\Big|_{x\ll g} \\ &= -CV_{\rm bias}^2 \end{aligned} \tag{9}$$

where C is the net capacitance.

The energy stored in the dielectric layers should not be ignored since it is also dependent on the displacement x of the structure. The expression for the electrostatic energy that is present within the capacitor (two oxides and air gap) is then obtained as follows:

$$\begin{aligned}U_{\rm fields} = \frac{1}{2}\epsilon_o\mathcal{E}_{\rm gap}^2\left((g-x)A\right) \\ + \left(\frac{1}{2}\epsilon_{\rm ox}\mathcal{E}_{\rm ox1}^2 + \frac{1}{2}\epsilon_{\rm ox}\mathcal{E}_{\rm ox2}^2\right)(At_{\rm ox}).\end{aligned} \tag{10}$$

As described previously, the total energy in the system is $U_{\rm sys} = U_{\rm fields} + (U_V^0 + \Delta U_V)$. Since the gradient of $U_{\rm sys}$ gives the force on the capacitor plates, we can use $F_{\rm beam} = -\nabla_x U_{\rm sys}$ to obtain the force on the resonator beam due to this one capacitor

$$F_{\rm beam}(x) = \frac{A\epsilon_o(V_{\rm bias}\epsilon_{\rm ox} + t_{\rm ox}\left(\rho_{s1}-\rho_{s2}\right))^2}{2\left(2t_{\rm ox}\epsilon_o + (g-x)\epsilon_{\rm ox}\right)^2}. \tag{11}$$

The total electrostatic force on the resonator beam considering capacitors on both sides acting in opposition to each other is given by

$$F_e = F_{\rm beam}(x) - F_{\rm beam}(-x). \tag{12}$$

We can linearize this force expression using the first-order terms of the Taylor expansion around $x \approx 0$ and obtain the following expression:

$$F_e = 2x\frac{A\epsilon_o\epsilon_{\rm ox}^3\left(V_{\rm bias} + \frac{t_{\rm ox}}{\epsilon_{\rm ox}}(\rho_{s1}-\rho_{s2})\right)^2}{(2t_{\rm ox}\epsilon_o + g\epsilon_{\rm ox})^3}. \tag{13}$$

This is a displacement-dependent force contribution due to the charge and the applied voltage, which is similar to the one caused due to the bias voltage alone. The spring is ignored in this analysis since we seek an electrostatics-related correction to the spring constant (indicated by the subscript in F_e).

To obtain the effective spring constant of the resonator, we use $k = \partial F/\partial x$. Performing this operation on the total force $F = F_k + F_e$ yields $\partial F/\partial x = k_m - k_e$, where k_m is the spring constant from the mechanics alone and k_e is a correction coming from the electrostatic effects. This electrostatic spring constant correction (softening) in the presence of both charge and voltage is then given by

$$k_e = \frac{2A\epsilon_o\epsilon_{\rm ox}^3\left(V_{\rm bias} + \frac{t_{\rm ox}}{\epsilon_{\rm ox}}(\rho_{s1}-\rho_{s2})\right)^2}{(2t_{\rm ox}\epsilon_o + g\epsilon_{\rm ox})^3}. \tag{14}$$

The experimentally observable frequency f_o' is then obtained through a linearized model

$$f_o' = \frac{1}{2\pi}\left(\frac{k_m - k_e}{m}\right)^{1/2} \approx f_o\left(1 - \frac{k_e}{2k_m}\right) \tag{15}$$

where

$$f_o = \frac{1}{2\pi}\sqrt{\frac{k_m}{m}} \tag{16}$$

is the mechanical resonance frequency in the absence of charge and bias effects, and is also described in [26]. Here, m is the effective mass of the resonator.

We can confirm the applicability of (14) to a special case where there is no oxide. For this, we set $\epsilon_{\rm ox} = \epsilon_o$, $t_{\rm ox} = 0$, and the charges $\rho_{s1} = \rho_{s2} = 0$. The spring-softening result is then

$$k_e\big|_{\rm no\,oxide} = \frac{2\epsilon_o AV_{\rm bias}^2}{g^3}. \tag{17}$$

This result is often seen in derivations of an electrostatic spring-softening although bias voltage.

C. Bulk-Charge Model

The aforementioned derivation only considers a surface charge on the oxide–vacuum interface. It is straightforward to modify this analysis for arbitrarily placed charge sheets ρ_{s1} and ρ_{s2} within the oxide layer, at positions x_1 and x_2 from their respective oxide–silicon interfaces (Fig. 4). The resulting spring-softening contribution due to both the charge and the applied voltage is then given by the following expression:

$$k_e = \frac{2A\epsilon_o\epsilon_{\rm ox}^3\left(V_{\rm bias} + \frac{1}{\epsilon_{\rm ox}}(x_1\rho_{s1} - x_2\rho_{s2})\right)^2}{(2t_{\rm ox}\epsilon_o + g\epsilon_{\rm ox})^3}. \tag{18}$$

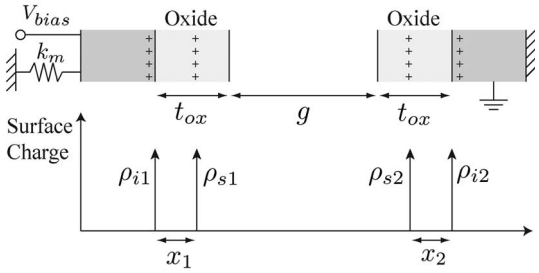

Fig. 4. Single-capacitor model for charge sheets that are placed at an arbitrary position within the dielectric layer for the analysis of the effects of bulk charge. Only one charge sheet is considered within each dielectric. The induced electrode charge retains its position at the oxide–electrode interface.

Mapping bulk-charge distributions in the dielectric to an equivalent surface charge is possible by integrating the spring-softening effects of the individual effective charge sheets over the dielectric bulk. In the case of RF capacitive switches, van Spengen *et al.* [29] extend the solution for an arbitrarily placed charge sheet within a single dielectric in a capacitive actuator to solve for the effects of bulk-charge distributions, and Rottenberg *et al.* [33] explain how bulk-charge distributions can be mapped to equivalent surface charges.

D. Predictions From the Model

1) Built-In Voltage: The charge state given by ρ_{s1} and ρ_{s2} in (14) can conveniently be expressed as a built-in voltage

$$V_{\rm bi} = \frac{t_{\rm ox}(\rho_{s1} - \rho_{s2})}{\epsilon_{\rm ox}} \tag{19}$$

yielding

$$k_e = \frac{2A\epsilon_o\epsilon_{\rm ox}^3}{(2t_{\rm ox}\epsilon_o + g\epsilon_{\rm ox})^3}(V_{\rm bias} + V_{\rm bi})^2. \tag{20}$$

The prefactor of the aforementioned expression is only dependent on geometry and material properties and is a constant for a given resonator design. It is valuable to emphasize that the built-in voltage does not depend on the mechanical properties of the resonator and is merely a function of charge state, oxide thickness, and dielectric constant. This built-in voltage effect has been described previously by the RF MEMS community [28] for its effects on actuation force in parallel plate actuators with dielectric on one electrode. Several detailed models [29], [33] have been established for these devices.

This built-in voltage should then affect frequency in a manner that is similar to the applied bias voltage in its spring-softening contribution. For instance, when $V_{\rm bi} > 0$ and $V_{\rm bias} > 0$, we have $(V_{\rm bias} + V_{\rm bi})^2 > (-V_{\rm bias} + V_{\rm bi})^2$. This relation in addition to (20) leads to

$$k_e\big|_{\text{positive bias}} > k_e\big|_{\text{negative bias}} \tag{21}$$

and, thus, the frequency for positive bias is lower than the frequency of negative bias of the same magnitude. When $V_{\rm bi} < 0$, we can expect to see

$$k_e\big|_{\text{positive bias}} < k_e\big|_{\text{negative bias}} \tag{22}$$

leading to a higher positive bias frequency instead. This asymmetry in frequency caused through the built-in voltage can be seen in the experimental observations shown in Fig. 5.

Moreover, $V_{\rm bi}$ should not be confused with the diode junction potential based on work-function (or Fermi level) differences between two differently doped regions of a semiconductor.

2) Measurement of Charge: Since the bias-frequency dependence of a resonator is analytically predictable based on the design of the resonator, it should be possible to back calculate how much charge is located on the resonator oxides simply from measuring a single frequency at a single bias voltage. However, such predictions are generally poor since they assume entirely predictable and accurate as-manufactured geometries and material properties.

As an alternative, the result can be obtained through curve fitting of the frequency-versus-bias-voltage curve, where the exact resonator frequency and dimensions, spring constant, electromechanical gaps, and oxide thickness are unknown but assumed constant. All of those unknown properties in k_e can be lumped together into a single unknown constant term ξ

$$\begin{aligned} f_o' &= f_o\left(1 - \frac{k_e}{2k_m}\right) \\ &= f_o\left(1 - \xi(V_{\rm bias} + V_{\rm bi})^2\right). \end{aligned} \tag{23}$$

The unknowns f_o, ξ, and $V_{\rm bi}$ can be fitted using any numerical analysis technique since $V_{\rm bias}$ is the input variable and f_o' is the observed frequency output from the system. As it has also been described in [26], f_o should be the mechanical resonance frequency in the absence of electrostatic spring softening and is a fixed number for a given resonator under constant environmental conditions. This also implies that a given built-in voltage $V_{\rm bi}$ will cause different magnitude effects on frequency for different resonator designs. Thus, resonators can be designed for increased sensitivity to charge buildup for use as sensors or with decreased sensitivity for use as stable frequency references (discussed in Section III-D3).

Finally, the surface charge equivalent of the built-in voltage can be extracted through (19). For instance, for a $t_{\rm ox} = 0.4$ μm thick silicon dioxide layer, $V_{\rm bi} = 100$ mV corresponds to about $\rho_{s1} - \rho_{s2} = 9 \times 10^{-10}$ C/cm^2 or about 5.6×10^9 charges/cm^2. As we will show later in Section IV-B, the amount of fixed voltage that we observe on our devices is of a similar order (expressed in voltage). These numbers compare well to the interface charge densities of the order 10^{11} charges/cm^2 in thermal silicon dioxide as reported in semiconductor literature [34]–[36]. It is thus reasonable to hypothesize that the built-in voltage is caused due to a few percent difference in the charge states on the resonator beam and electrode oxides.

In certain cases, the previously described fitting technique can be inadequate due to the appearance of other electromechanical frequency effects that have not been modeled here, such as spring nonlinearity due to large amplitude actuation. In such cases, the data may not fall on a quadratic curve described by (23). However, the built-in voltage can be extracted by translating the frequency–bias-voltage data along the voltage axis to create a symmetric curve about the frequency axis. The

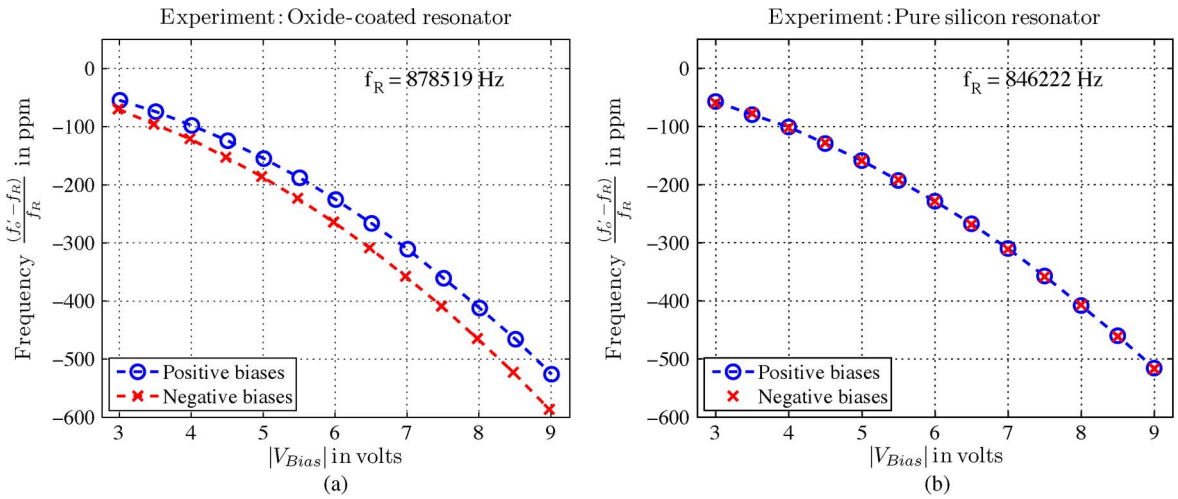

Fig. 5. Experimental data show the effects due to built-in voltage $V_{\rm bi}$. The quadratic dependence of frequency on bias voltage is seen. In oxide-coated devices, the bias-frequency curves depend on bias polarity, indicating the effect of built-in voltage, whereas the frequency is independent of bias polarity for silicon-only resonators. The data are taken using the sweep setup described in Section IV-A. The f_R in each case is the extrapolated zero bias frequency to which the data are normalized for visualization. (a) Sample data from an oxide-coated resonator. (b) Sample data from a pure silicon resonator.

amount of translation along the voltage axis required to do this is the built-in voltage.

3) Charge Sensitivity: An important metric for the stability of frequency references is the fractional change in frequency over time. If the charge state $V_{\rm bi}$ changes over time, the frequency will drift as well. Continuing from (23), the fractional frequency sensitivity to charge (mapped to built-in voltage $V_{\rm bi}$) is

$$\frac{1}{f_o}\frac{\partial f_o'}{\partial V_{\rm bi}} = -2\,\xi\,(V_{\rm bias}+V_{\rm bi}) \approx -2\,\xi\,V_{\rm bias} = -\frac{V_{\rm bias}}{k_m}\frac{2A\epsilon_o\epsilon_{\rm ox}^3}{(2t_{\rm ox}\epsilon_o+g\epsilon_{\rm ox})^3} \quad (24)$$

when $V_{\rm bi}$ is a small change in voltage around the $V_{\rm bias}$ operating point.

We can see that, to build more stable frequency references, we should create stiffer resonators (higher k_m) that operate at lower bias voltages. Increasing the electrostatic gap g and decreasing the actuation area A should also make the device less sensitive to frequency variations due to charge. Increasing the oxide thickness $t_{\rm ox}$ may also help; however, the $g\epsilon_{\rm ox}$ term is typically dominant in the denominator for our resonators.

The result in (24) is identical to the bias-frequency sensitivity of the structure. This is correct since the charge acts on the resonator through a change in the effective bias voltage.

4) Frequency Behavior During Charge Drift: The expression of built-in voltage $V_{\rm bi}$ can be extracted from the bulk-charge model (18) as

$$V_{\rm bi} = \frac{(x_1\rho_{s1}-x_2\rho_{s2})}{\epsilon_{\rm ox}}. \quad (25)$$

Starting from steady state, for positive ρ_{s1} and under positive biasing $V_{\rm bias}>0$, we can expect a motive force on the charge sheet ρ_{s1} toward the surface of the dielectric away from the silicon [Fig. 6(a)]. Then, we note that the built-in voltage $V_{\rm bi}$ increases in magnitude due to this motion of charge (x_1 is

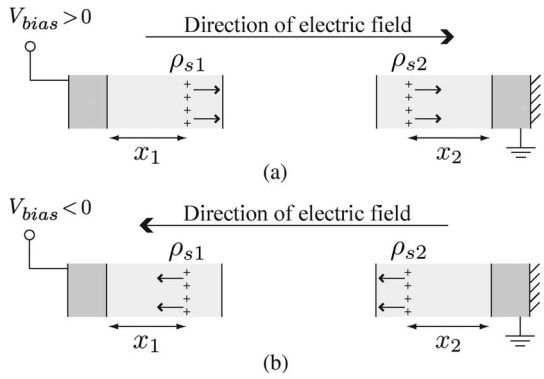

Fig. 6. Explaining drift of frequency under positive and negative bias voltage by using the charge sheet model (Section III-C). The drift of the charge affects $V_{\rm bi}$ through (25) and causes a change in frequency. (a) Charge drift under positive biasing of the resonator. (b) Charge drift under negative biasing of the resonator.

increasing) over time. As a result, the net effective bias voltage $(V_{\rm bias}+V_{\rm bi})$ increases, and the frequency goes down over time (since spring softening is increased). If ρ_{s2} is also positive, it is seen that, under positive bias, this charge sheet moves toward the silicon [Fig. 6(b)] and causes less of an effect on the frequency (since x_2 is decreasing). However, this reduced contribution of $x_2\rho_{s2}$ increases $V_{\rm bi}$ and decreases the frequency as well. The net effect due to the motion of ρ_{s1} and ρ_{s2} is the transient reduction of the frequency.

A similar argument is made in the case of negative biasing, where it is observed that $V_{\rm bi}$ decreases over time. However, this still increases the magnitude of the effective bias voltage since $V_{\rm bias}<0$ in this case. Thus, even under negative biasing, the frequency is expected to decrease.

The effect described earlier is observed and is described in Section IV-C. It must be stated that this charge sheet model is not realistic but allows us to intuitively understand the dynamic effects of charge in the system. Positive charge sheets were used for illustration in the aforementioned discussion, but the result is identical if a negative charge is used instead. The frequency

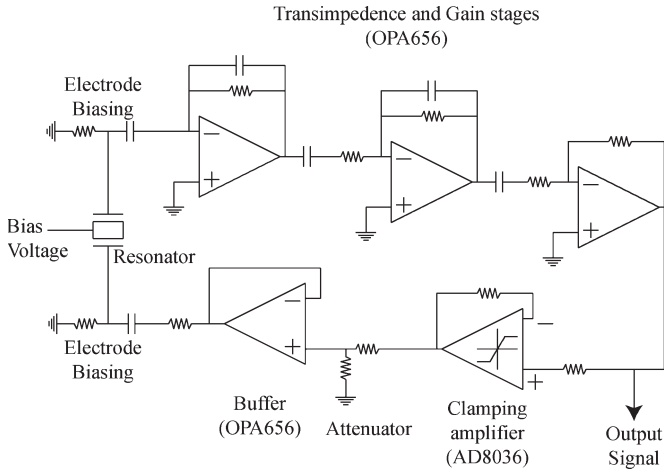

Fig. 7. Oscillator circuit schematic. The resonator output is amplified through a series of Texas Instruments OPA656 operational amplifiers acting as transimpedance and gain stages with some filtering characteristics for improved signal-to-noise ratio. The oscillator output is obtained at the end of these stages. The signal is then clamped to limit power (using an Analog Devices AD8036 wide-bandwidth clamping amplifier) and sent back to the resonator to create a positive feedback loop to sustain oscillations.

is expected to decrease as charge redistributes over time under constant applied bias voltage, irrespective of its polarity.

IV. Results

A. Electrical Scheme and Experimental Method

The anchor is connected to a fixed bias voltage supply (typically 4–40 V depending on the resonator design and requirements). The stimulus and sense electrodes are held at the dc ground; however, they do carry the small millivolt-level ac resonance signal. In the theoretical analysis, the ac signal is assumed to be small enough to be negligible. The electrical connections were shown previously in Fig. 1.

Experiments are performed in a stabilized oven equipped with a Thermotron S1.2C temperature controller for removing temperature variations in the resonator frequency. In any given experiment, the temperature is kept constant. In most cases, it is set to around 40 °C and is controlled within ± 0.1 °C. The bias voltage is controlled using a Valhalla 2701C voltage calibrator to a stability that is better than 1 mV in order to eliminate variations due to bias voltage noise or bias drift.

In frequency sweep experiments, the resonator is placed inside the oven. An ac stimulus signal is provided by a network analyzer, and the output of the resonator is connected back to the analyzer through a transimpedance amplifier. The resonance peak is tracked in the frequency domain. To obtain a single data point using this method, it takes a time of up to a few minutes per resonator depending on the analyzer settings (for accuracy). The high quality factor allows for a fairly good (± 5 ppm) accuracy in determining the frequency.

In oscillator experiments, the resonators are connected to individual oscillator boards inside the oven. The oscillator schematic is shown in Fig. 7. The frequency output of the oscillator is monitored with an Agilent 53132A universal frequency counter equipped with a built-in high-stability reference to get a sub-parts-per-million accuracy. The frequency is thus tracked in the time domain. The time taken for each frequency data point using this technique is on the order of 2 s, which is mostly due to general-purpose interface bus (GPIB) overhead. As a result, faster variations in frequency can be better tracked using this method in contrast to frequency-domain sweep testing. The use of oscillators enables very high resolution real-time observation of charge motion.

B. Fixed Oxide Charge

The frequency of the resonant peak is monitored for various bias voltages using the sweep setup as described in Section IV-A. These frequency data are then plotted against the magnitude of the applied bias as was done previously in Fig. 5. For a device that is free of any built-in voltage, the positive- and negative-polarity bias-frequency curves should overlap exactly. For a device that has a nonzero built-in voltage, the resonant frequency will be bias polarity dependent. Collecting these frequency-versus-bias-voltage data allows us to fit to the model described in Section III-D 2 and extract the built-in voltage $V_{\rm bi}$.

The extracted built-in voltages of the devices from three wafers representing wet oxide, dry oxide (Section II-C), and silicon-only devices are shown in Fig. 8. The lack of any apparent built-in potential in pure silicon resonators (Table I) indicates that there is little or no oxide or charge in these devices. As such, these silicon-only resonators are excellent for frequency stability experiments [5].

Oxide-coated resonators show a measurable built-in voltage. It must be noted from (19) that a built-in voltage will only appear in an oxidized device when there is a difference in the charge distribution between the two electrodes of the equivalent capacitor, i.e., between the resonator beam and the drive/sense electrodes. The presence of a built-in voltage indicates that there is an imbalance in the charge state of the oxides on the two sides since $V_{\rm bi} = 0$ if $\rho_{s1} = \rho_{s2}$. The reasons for this observed charge imbalance are not presently well understood.

We note from Table I that wet-oxidized devices, on average, seem to have a negative built-in voltage ($\mu = -51$ mV); however, large standard deviation is seen ($\sigma = 130$ mV). Dry thermal oxide devices seem to have a more balanced charge distribution across the device electrodes, resulting in lower built-in voltages ($\mu = +23$ mV) and a narrower spread ($\sigma = 21$ mV). As long as this built-in potential keeps a fixed value, it is acceptable to use these devices for stable frequency references since they will not drift over time.

C. Mobile Oxide Charge

Mobile charge in oxide-coated resonators is observed using the oscillator setup described in Section IV-A in order to capture fast features in the data and to achieve higher resolution than the sweeping method used in Section IV-B and in [25].

Although silicon devices do not contain dielectrics that can charge up and affect frequency, they are still affected by bias voltage and temperature effects during experiments. Since these dependences on bias and temperature are well known, these resonators are used as references throughout the following experiments to compare against the performance of oxidized

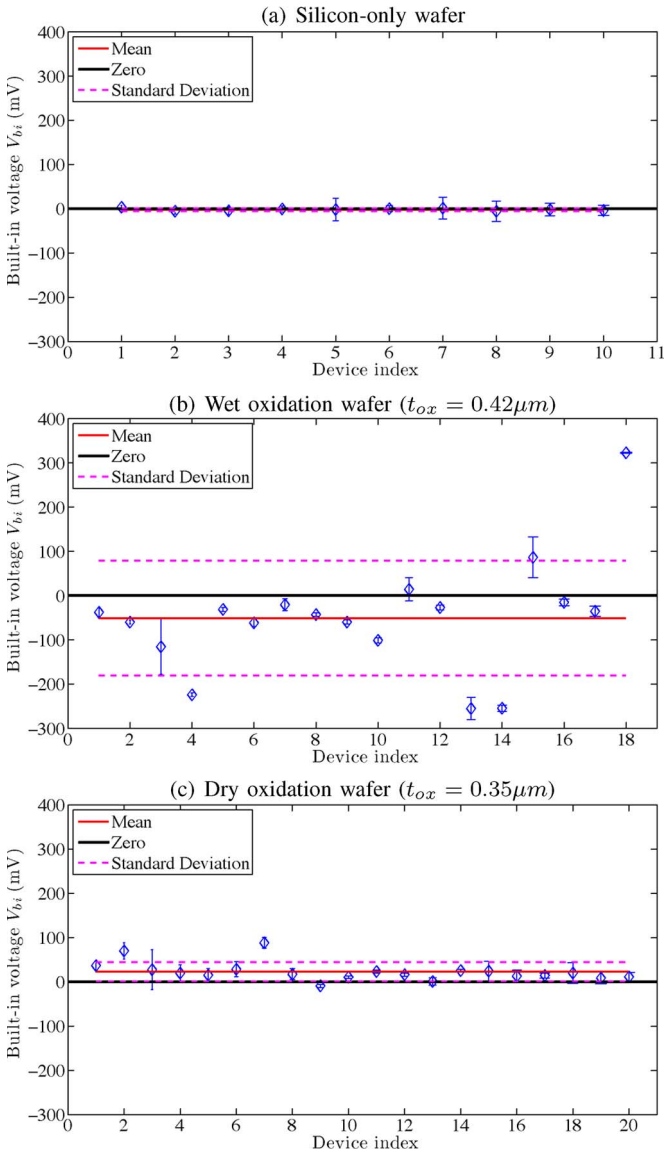

Fig. 8. Built-in voltage $V_{\rm bi}$ observed in the test wafers. The data are plotted on identical vertical scales in order to visualize the difference between the wafer types. The device index is arbitrary and indicates the $V_{\rm bi}$ values obtained from individual resonators. The statistics are enumerated in Table I.

TABLE I
STATISTICS OF BUILT-IN VOLTAGE $V_{\rm bi}$ FROM THE DATA SHOWN IN FIG. 8

Wafer Type	V_{bi} Mean μ	V_{bi} Std. Dev. σ
Silicon only	- 1.8 mV	3 mV
Wet oxidation 0.45 μm	- 51 mV	130 mV
Dry oxidation 0.36 μm	+ 23 mV	21 mV

resonators on the same bias voltage supply and in the same temperature-stabilized oven.

The following mobile charge observations are performed with resonators found on the wet-oxidation wafer with the oscillator testing setup. As a point of reference, when a 20-V bias is applied across a charge-free device that has transduction gap features $g = 1.1$ μm and $t_{\rm ox} = 0.4$ μm, the electric field strengths are estimated to be $\mathcal{E}_{\rm ox1} = \mathcal{E}_{\rm ox2} = 3.9 \times 10^4$ V/cm and $\mathcal{E}_{\rm gap} = 1.5 \times 10^5$ V/cm. The actual field strengths depend

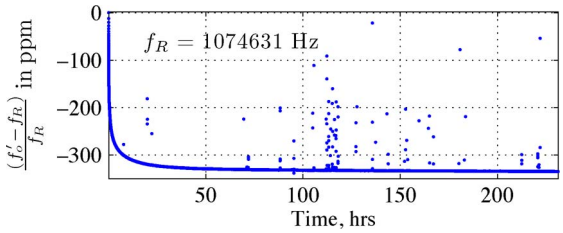

Fig. 9. Long-duration frequency (f_o') observation of a wet-oxidized resonator operating under constant bias and temperature conditions in an oscillator. The resonator shows a large decreasing frequency transient over many hours. The stray data points are created when occasional noise sources cause additional zero crossings in the signal going to the frequency counter.

on both the applied bias voltage and the charge state of the dielectrics. As a point of comparison, the field strength in the dielectric of a MOSFET built in the 45-nm technology node [37] can be estimated to be around 10^7 V/cm.

1) Initial Observations: Of the 17 devices from the wet-oxidation wafer that were tested for drift, two resonators exhibit large decreasing frequency transients ($>$ 50 ppm decrease) over short durations ($\sim$1 h) immediately after the bias voltage is changed (shown in Fig. 9). These transients are the focus of the mobile charge study.

The remaining 15 devices that were tested do not have this short-term transient behavior. Of these, five devices have shown both increasing and decreasing transients of small magnitude ($<$ 10 ppm) over very short durations (a few minutes). Such quick-settling transients are of low importance if a short burn-in period is acceptable to the application. These oxidized devices are usable for frequency stability experiments as demonstrated by Salvia *et al.* [38] and Lee *et al.* [39]. It must be noted, however, that these resonators have not been characterized over long periods of time, and frequency drifts on the order of a few parts-per-million per week have occasionally been observed. Additional supporting long-term data with a different set of devices have been shown through sweep testing by Melamud *et al.* [25], where it is noted that 12 out of 14 devices tested showed frequency stability within $\pm$2 ppm over a testing duration of 200 days. This result shows promise for long-term frequency stability while demonstrating that a small number of poorly performing devices do exist.

This drift behavior is absent in the silicon-only resonators, and they show stable frequency under constant temperature and biasing conditions.

Action of the bias voltage supply cannot account for the observed drifts in frequency since the time constants observed are too large. In addition, the supply's voltage accuracy error is too small to explain the transient through the bias-frequency sensitivity of the devices. Although the temperature is kept constant in a stabilized oven environment, there are still some random fluctuations that affect the frequency. Since the resonators are passively temperature compensated with the oxide [9], temperature fluctuations of $\pm$0.1 °C can only account for frequency variations that are less than $\pm$3 ppm at the operating temperature of 40 °C on the specific devices presented here. The oscillator circuit boards are reusable and are often exchanged between devices to ensure that any drifts and transients are not oscillator artifacts.

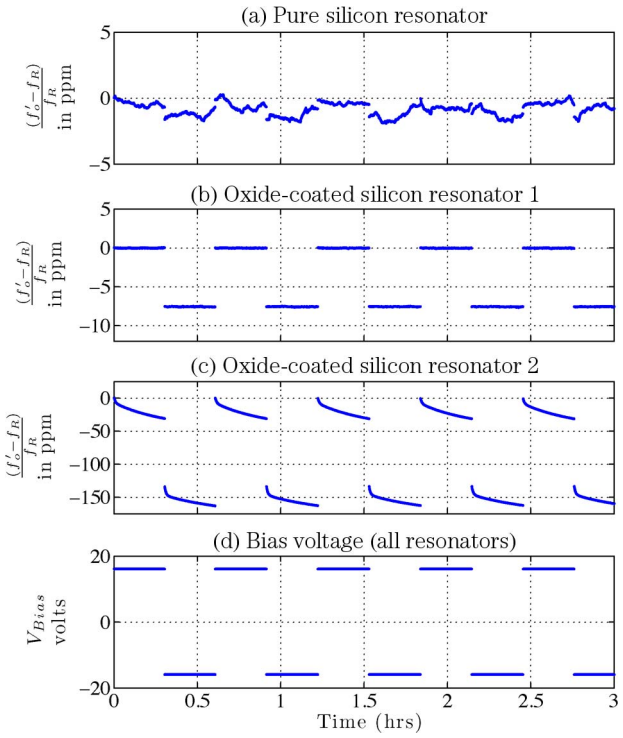

Fig. 10. Behavioral comparison of lithographically identical resonators. The data for each resonator are normalized to a different f_R that is the first point of each data set. The two oxide-coated devices (b) and (c) are taken from the same wafer, while the silicon device (a) was on a different silicon-only wafer not taken through the oxidation treatment. The high zoom in the silicon resonator data shows temperature effects. This temperature variation is much smaller in the oxide-coated resonators since they are passively temperature compensated.

Since the analysis of the present devices is complicated by the fact that oxide coats all exposed silicon surfaces within the encapsulation, charges on or within these oxides may also affect the resonator's behavior. Additional experiments with selective or localized oxide coatings, annealing treatments to improve oxide quality, gettering agents to arrest mobile charge carriers, or conductive coatings to neutralize charge could help to better understand and model the charging behavior.

2) Variability: Fig. 10 shows the frequency trends of three resonators as the bias is alternated between +18 and −18 V with a 50% duty cycle. The three devices are lithographically identical. The two oxidized resonators are taken from the same wafer. All resonators were placed in an oven together and share the same bias voltage supply.

The bias-polarity dependence of frequency is visible in the data from both oxide-coated resonators, indicating a built-in voltage. This is not caused due to magnitude inaccuracy in the bias supply since the silicon resonator does not show this effect, and the bias-frequency dependence of all three resonators is very similar.

In addition, the oxide-coated resonator in Fig. 10(c) shows a repeatable transient behavior in time. It has been observed previously for RF capacitive switches that bipolar actuation waveforms still lead to net drift of device characteristics due to charging [40], [41]. It is not yet certain whether this is the case in our devices as well.

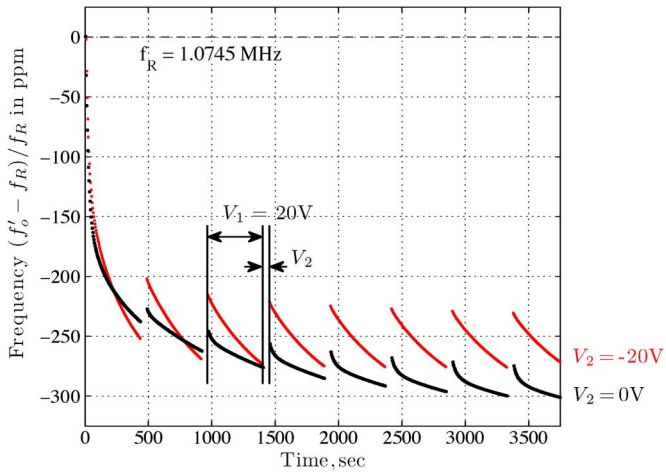

Fig. 11. Demonstrating the effect of non-50% duty cycle bipolar biasing. Frequency recovery under zero bias is also observed.

Both the built-in voltage and frequency transient effects are absent in silicon resonators as evidenced by the silicon device in Fig. 10(a). The aforementioned observations indicate that these effects are due to the presence of the oxide.

3) Bias-Voltage Dependence: Reproducibility of the short-duration transients (shown in Fig. 10) in oxide-coated resonators strongly indicates that shape change, fatigue, pressure change, adsorption and desorption of gases, and other burn-in processes or material issues can be ruled out.

The transient behavior of frequency can be controlled using various bias alternation schemes. In the experiment shown in Fig. 11, two bias voltages are used with a different duty cycle. The device is allowed to drift under a +20-V bias voltage for 90% of the bias cycle, and −20 V is applied for the remaining 10% cycle to attempt to move the charge back toward the initial state. We see that the frequency recovers to the previous values when observed at +20 V after the momentary application of this negative bias voltage. However, since the duty cycle for the biases is unequal, we see an overall tendency for the frequency to drift preferentially in one direction. This is expected if we assume that charging and discharging processes take place at similar rates.

Note that, even when zero bias is applied for the 10% portion of the bias cycle, we still see some frequency recovery (Fig. 11). This is an important observation, as it suggests that there is a self-recovery process acting within the system that does not require the presence of an externally applied electric field. The source of this recovery effect can be speculated as a diffusion process possibly assisted by the field generated by the diffusing charged species themselves. Similar observations of unbiased device recovery have been made previously for nonresonant capacitive actuators [28], [41]. In the case of resonators, this recovery effect cannot be directly observed when no bias voltage is applied since the sensing is performed through electrostatic transduction. At low bias voltage, the motional impedance of the resonator is too high, and the frequency peak disappears below the noise. This effect can, however, be explored by looking at the device behavior under varied magnitude biases of the same polarity as done in the following experiment.

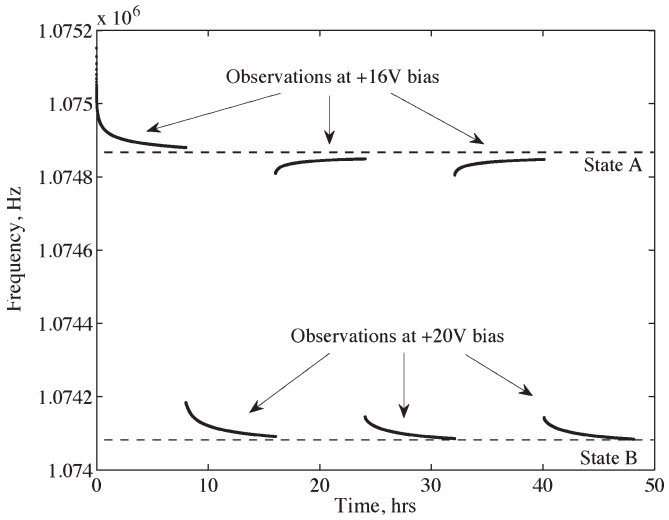

Fig. 12. Exploring the driving forces on charge motion through biasing experiments. The "upward" transients in the +16-V observations indicate that the electric field is not the only driving force on the charge.

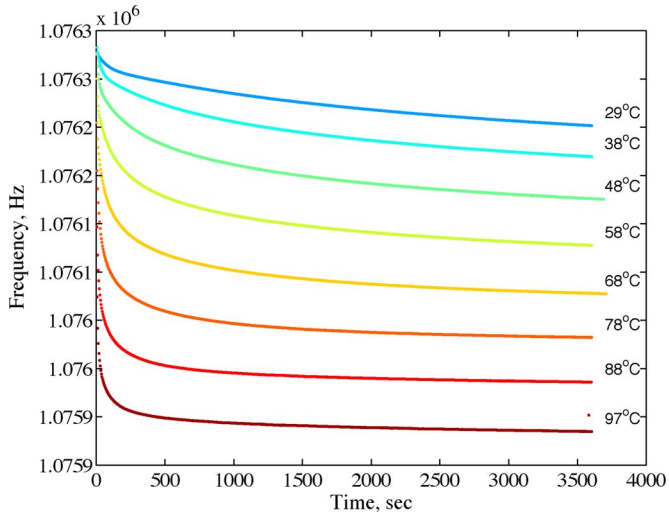

Fig. 13. Observation of frequency transients accelerating with increasing temperature. Note that the x-axis has an arbitrary time origin for each data set since they are acquired at different times from the same resonator.

In the oscillator experiment shown in Fig. 12, the bias is alternated between two voltages with a 50% duty cycle. The frequency is first allowed to drift under a positive 16-V bias voltage reaching close to a final state A. This is interpreted as the drift of a charge within the dielectric in the presence of an electric field, and it is consistent with the explanation given in Section III-D4. When the frequency transient has significantly diminished, the bias voltage is increased to 20 V, which increases the electric field in the transduction gap. This increase of the bias has the following two effects: 1) The frequency reduces instantly based on the spring-softening effect, and 2) the transient in the frequency reappears and eventually brings the system to state B. The reappearance of a frequency transient indicates an increase in $V_{\rm bi}$ to reach a new equilibrium beyond that of state A. When the field is reduced by reducing the applied bias back to 16 V, the oscillator frequency is observed moving in the opposite direction back toward state A. The direction of this transient indicates that $V_{\rm bi}$ is decreasing over time, although the applied electric field is still in the same direction (since bias polarity was maintained). It must then be concluded that the applied electric field is no longer the dominant driving force on the charge and that this motion of the charge is occurring under some other influence. It is seen that this back and forth movement between two steady states A and B happens consistently as the bias is alternated in this manner.

4) Temperature Dependence: A preliminary investigation of the effects of temperature has also been performed. Frequency transients appear to accelerate with increasing temperature, as shown by the representative data set in Fig. 13. Extraction of a single time constant for these trends is not meaningful since the curves do not agree with a single exponential function [28]. However, the extraction of empirical curve fits is useful for the description of the data for engineering purposes. Two exponentials of the form

$$f_o' = f_o + A_1 e^{-t/\tau_1} + A_2 e^{-t/\tau_2} \tag{26}$$

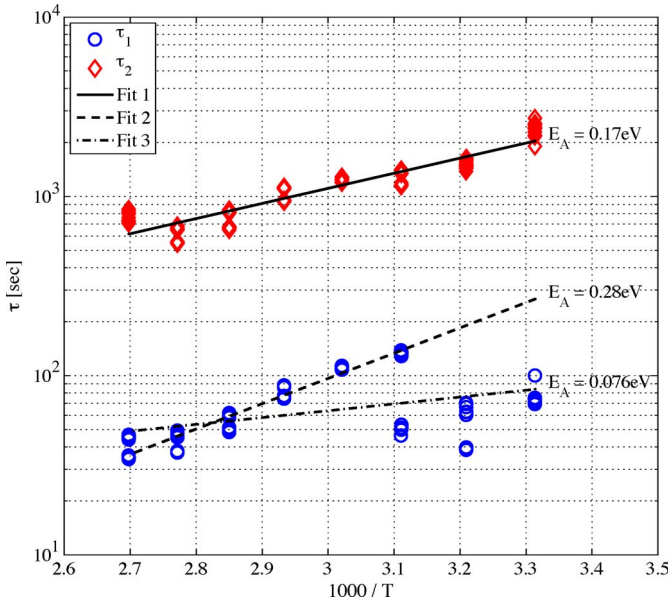

Fig. 14. Extraction of time constants from 96 observations of resonator frequency drift against time. The data are fitted to the transient curves as described by (26), and the time constants are presented as a function of temperature T. The linear fits are used to extract the activation energy according to $\tau = \tau_o \exp(-E_A/kT)$. Fits 1 and 3 incorporate all the data, while fit 2 disregards the lower right side "stray" data points in τ_1. These points are suspected to be a fitting artifact due to poor agreement with the fitting function in the initial part of the drift characteristic.

have been found to be adequate for describing the data, although the curve fit visibly improves once a third decaying exponential term is added to the previous expression. The two time constants in (26) have been extracted by nonlinear least square fitting for a large set of trials. They are presented in Fig. 14 in the form of an Arrhenius plot.

Similar trends have been seen previously in RF MEMS switches [42], where stretched exponential curves were used to fit the capacitance transients seen during dielectric polarization. Stretched exponentials have been widely used in scientific literature to describe processes where a distribution of time

constants can be expected. We attempted to fit our data to a similar stretched exponential curve of the form

$$f_o' = f_o + A_1 e^{-(t/\tau_1)^\beta} \tag{27}$$

but noted that the value of β is not constant across temperature. Since the result of curve fitting to (27) is visibly no better than the fit to (26), we decided to stay with the two-exponential description.

The acceleration of the frequency transients with increasing temperature is consistent with the concept of increased mobility of charge-carrying species (ions and protons) within dielectrics at higher temperatures [43].

V. Conclusion

Passive temperature compensation of resonators using SiO_2 coatings is a very effective technology for enabling high-stability frequency references. However, the technique is hindered by a charge appearing within the dielectric in the transduction gap and affecting system properties. We have presented an electrostatics-based model for the effects of such charge on resonator frequency. Frequency-versus-bias-voltage measurements are consistent with the developed model and thus help to infer the presence of charge in the thermally grown silicon dioxide dielectric in our resonators. Based on built-in charge observations from multiple devices, we have noted that dry thermal oxides show lower fixed charge (with lower standard deviation) than wet thermal oxides.

Short-duration transient drifts in the frequency of large magnitude have been observed in a small set of oxidized devices. The direction of these drifts can be explained qualitatively based on the model. In these cases, the transient behavior is repeatable and reversible and shows a strong bias dependence as well as a strong temperature dependence, indicating the presence of mobile charge. In a majority of devices (15 of 17), however, these large transients are absent. Although the long-term stability of these devices for frequency reference applications is yet to be established, they have already been used successfully by Salvia *et al.* [38] and Lee *et al.* [39] for demonstrating active frequency compensation techniques. A 2-ppm resolution-limited bound for stability was established by Melamud *et al.* [25] in a majority of devices (12 of 14) tested in a parallel study.

The effects of fixed charge in a resonator are possible to calibrate out of the system. Mobile charge, however, needs to be controlled or predicted since it can affect frequency during the operation of the device. Since a majority of our oxide-coated test devices do not show significant drifts in frequency, there is still much promise for applying oxide compensation technology to frequency references.

Acknowledgment

The authors would like to thank G. Yama, H. Lee, Y. Q. Qu, S. Yoneoka, Dr. C. M. Jha, Prof. C. Nguyen, Dr. A. Partridge, M. Lutz, and Dr. E. Perozziello for their guidance and support. Additional support was provided in part by a National Science Foundation Graduate Fellowship for J. C. Salvia, and in part by a Stanford Graduate Fellowship for Dr. R. Melamud. This work was performed at the Center on Interfacial Engineering for Microelectromechanical Systems.

References

[1] G. Bahl, R. Melamud, B. Kim, S. Chandorkar, J. C. Salvia, M. Hopcroft, R. Hennessy, S. Yoneoka, C. Jha, G. Yama, D. Elata, R. Candler, R. Howe, and T. Kenny, "Observations of fixed and mobile charge in composite MEMS resonators," in *Proc. IEEE Int. Conf. Solid-State Sens., Actuators, Microsyst.*, Hilton Head Island, SC, Jun. 1–5, 2008, pp. 102–105.

[2] M. Lutz, A. Partridge, P. Gupta, N. Buchan, E. Klaassen, J. McDonald, and K. Petersen, "MEMS oscillators for high volume commercial applications," in *Proc. IEEE Int. Conf. Solid-State Sens., Actuators, Microsyst.*, Jun. 2007, pp. 49–52.

[3] W. Hsu, J. Clark, and C. Nguyen, "Mechanically temperature-compensated flexural-mode micromechanical resonators," in *IEDM Tech. Dig.*, San Francisco, CA, 2000, pp. 399–402.

[4] W.-T. Hsu and C.-C. Nguyen, "Stiffness-compensated temperature-insensitive micromechanical resonators," in *Proc. 15th IEEE Int. Conf. Microelectromech. Syst.*, Las Vegas, NV, 2002, pp. 731–734.

[5] M. A. Hopcroft, B. Kim, S. Chandorkar, R. Melamud, M. Agarwal, C. M. Jha, G. Bahl, J. C. Salvia, H. Mehta, H. K. Lee, R. N. Candler, and T. W. Kenny, "Using the temperature dependence of resonator quality factor as a thermometer," *Appl. Phys. Lett.*, vol. 91, no. 1, p. 013 505, Jul. 2007.

[6] K. Sundaresan, G. Ho, S. Pourkamali, and F. Ayazi, "Electronically temperature compensated silicon bulk acoustic resonator reference oscillators," *IEEE J. Solid-State Circuits*, vol. 42, no. 6, pp. 1425–1434, Jun. 2007.

[7] E. Quevy and R. Howe, "Redundant MEMS resonators for precise reference oscillators," in *Proc. RFIC Symp.*, 2005, pp. 113–116.

[8] B. Berry and W. Pritchet, "Temperature compensation for constant-frequency electromechanical oscillators," *IBM Tech. Dis. Bull.*, vol. 14, no. 4, pp. 1237–1238, Sep. 1971.

[9] R. Melamud, B. Kim, S. Chandorkar, M. Hopcroft, M. Agarwal, C. Jha, and T. Kenny, "Temperature-compensated high-stability silicon resonators," *Appl. Phys. Lett.*, vol. 90, no. 24, p. 244 107, Jun. 2007.

[10] R. Sandberg, W. Svendsen, K. Molhave, and A. Boisen, "Temperature and pressure dependence of resonance in multi-layer microcantilevers," *J. Micromech. Microeng.*, vol. 15, no. 8, pp. 1454–1458, Jun. 2005.

[11] F. Shen, P. Lu, S. O'Shea, K. Lee, and T. Ng, "Thermal effects on coated resonant microcantilevers," *Sens. Actuators A, Phys.*, vol. 95, no. 1, pp. 17–23, Dec. 2001.

[12] W. Pang, H. Yu, H. Zhang, and E. Kim, "Temperature-compensated film bulk acoustic resonator above 2 GHz," *IEEE Electron Device Lett.*, vol. 26, no. 6, pp. 369–371, Jun. 2005.

[13] T. Parker and M. Schulz, "Temperature stable surface acoustic wave delay lines with SiO_2 film overlays," in *Proc. Ultrasonics Symp.*, Milwaukee, WI, Nov. 11–14, 1974, pp. 295–298.

[14] G. Cambon, E. Adler, J. Attal, and W. Shahab, "Temperature effects on acoustic surface wave devices on silicon," in *Proc. Ultrasonics Symp.*, New Orleans, LA, Sep. 26–28, 1979, pp. 637–640.

[15] X. Yuan, S. Cherepko, J. Hwang, C. Goldsmith, C. Nordqusit, and C. Dyck, "Initial observation and analysis of dielectric-charging effects on RF MEMS capacitive switches," in *IEEE MTT-S Int. Microw. Symp. Dig.*, Fort Worth, TX, Jun. 6–11, 2004, vol. 3, pp. 1943–1946.

[16] D. Molinero, R. Comulada, and L. Castañer, "Dielectric charge measurements in capacitive microelectromechanical switches," *Appl. Phys. Lett.*, vol. 89, no. 10, p. 103 506, Sep. 2006.

[17] S. Melle, D. De Conto, M. L. D. Dubuc, K. Grenier, L. Bary, R. Plana, O. Vendier, J. Muraro, and J. Cazaux, "Modeling of the dielectric charging kinetic for capacitive RF-MEMS," in *IEEE MTT-S Int. Microw. Symp. Dig.*, Long Beach , CA, Jun. 12–17, 2005, p. 4.

[18] R. Herfst, H. Huizing, P. Steeneken, and J. Schmitz, "Characterization of dielectric charging in RF MEMS capacitive switches," in *Proc. IEEE Int. Conf. Microelectron. Test Struct.*, Mar. 2006, pp. 133–136.

[19] C. Goldsmith, J. Ehmke, A. Malczewski, B. Pillans, S. Eshelman, Z. Yao, J. Brank, M. Eberly, R. Co, and T. Dallas, "Lifetime characterization of capacitive RF MEMS switches," in *IEEE MTT-S Int. Microw. Symp. Dig.*, 2001, vol. 1, pp. 227–230.

[20] R. Candler, M. Hopcroft, B. Kim, W. Park, R. Melamud, M. Agarwal, G. Yama, A. Partridge, M. Lutz, and T. Kenny, "Long-term and accelerated life testing of a novel single-wafer vacuum encapsulation for MEMS resonators," *J. Microelectromech. Syst.*, vol. 15, no. 6, pp. 1446–1456, Dec. 2006.
[21] J. Lander and J. Morrison, "Low voltage electron diffraction study of the oxidation and reduction of silicon," *J. Appl. Phys.*, vol. 33, no. 6, p. 2089, Jun. 1962.
[22] A. Ishizaka and Y. Shiraki, "Low temperature surface cleaning of silicon and its application to silicon MBE," *J. Electrochem. Soc.*, vol. 133, no. 4, pp. 666–671, Apr. 1986.
[23] B. Kim, R. Candler, R. Melamud, M. Hopcroft, S. Yoneoka, H. Lee, M. Agarwal, S. Chandorkar, G. Yama, and T. Kenny, "Hermeticity and diffusion investigation in polysilicon film encapsulation for microelectromechanical systems," *J. Appl. Phys.*, vol. 105, no. 1, p. 013 514, Jan. 2009.
[24] B. Kim, R. Candler, M. Hopcroft, M. Agarwal, W. Park, and T. Kenny, "Frequency stability of wafer-scale film encapsulated silicon based MEMS resonators," *Sens. Actuators A, Phys.*, vol. 136, no. 1, pp. 125–131, May 2007.
[25] R. Melamud, S. A. Chandorkar, B. Kim, H. K. Lee, J. C. Salvia, G. Bahl, M. A. Hopcroft, and T. W. Kenny, "Temperature-insensitive composite micromechanical resonators," *J. Microelectromech. Syst.*, vol. 18, no. 6, pp. 1409–1419, Dec. 2009.
[26] S. Kalicinski, H. Tilmans, M. Wevers, and I. D. Wolf, "A new characterization method for electrostatically actuated resonant MEMS: Determination of the mechanical resonance frequency, quality factor and dielectric charging," *Sens. Actuators A, Phys.*, vol. 154, no. 2, pp. 304–315, Sep. 2009.
[27] H. Tilmans and R. Legtenberg, "Electrostatically driven vacuum-encapsulated polysilicon resonators. II: Theory and performance," *Sens. Actuators A, Phys.*, vol. 45, no. 1, pp. 67–84, Oct. 1994.
[28] J. Wibbeler, G. Pfeifer, and M. Hietschold, "Parasitic charging of dielectric surfaces in capacitive microelectromechanical systems (MEMS)," *Sens. Actuators A, Phys.*, vol. 71, no. 1/2, pp. 74–80, Nov. 1998.
[29] W. van Spengen, R. Puers, R. Mertens, and I. De Wolf, "A comprehensive model to predict the charging and reliability of capacitive RF MEMS switches," *J. Micromech. Microeng.*, vol. 14, no. 4, pp. 514–521, Jan. 2004.
[30] F. Bannon, J. Clark, and C. Nguyen, "High-Q HF microelectromechanical filters," *IEEE J. Solid-State Circuits*, vol. 35, no. 4, pp. 512–526, Apr. 2000.
[31] R. Howe and R. Muller, "Resonant-microbridge vapor sensor," *IEEE Trans. Electron Devices*, vol. ED-33, no. 4, pp. 499–506, Apr. 1986.
[32] K. Wang, A. Wong, and C. Nguyen, "VHF free–free beam high-Q micromechanical resonators," *J. Microelectromech. Syst.*, vol. 9, no. 3, pp. 347–360, Sep. 2000.
[33] X. Rottenberg, I. De Wolf, B. Nauwelaers, W. De Raedt, and H. Tilmans, "Analytical model of the DC actuation of electrostatic MEMS devices with distributed dielectric charging and nonplanar electrodes," *J. Microelectromech. Syst.*, vol. 16, no. 5, pp. 1243–1253, Oct. 2007.
[34] B. Deal, M. Sklar, A. Grove, and E. Snow, "Characteristics of the surface-state charge (Q) of thermally oxidized silicon," *J. Electrochem. Soc.*, vol. 114, pp. 266–274, 1967.
[35] K. Seo, S. Sharma, A. Yasseri, D. Stewart, and T. Kamins, "Surface charge density of unpassivated and passivated metal-catalyzed silicon nanowires," *Electrochem. Solid-State Lett.*, vol. 9, no. 3, pp. G69–G72, Jan. 2006.
[36] P. Balk, Ed., *The Si–SiO_2 System*. Amsterdam, The Netherlands: Elsevier, 1988.
[37] International Technology Roadmap for Semiconductors, 2004. [Online]. Available: http://public.itrs.net/
[38] J. C. Salvia, R. Melamud, S. A. Chandorkar, S. F. Lord, and T. W. Kenny, "Real-time temperature compensation of MEMS oscillators using an integrated micro-oven and a phase lock loop," *J. Microelectromech. Syst.*, to be published.
[39] H. Lee, M. A. Hopcroft, R. Melamud, B. Kim, J. C. Salvia, S. Chandorkar, and T. Kenny, "Electrostatic-tuning of hermetically encapsulated composite resonator," in *Proc. IEEE Int. Conf. Solid-State Sens., Actuators, Microsyst.*, Hilton Head Island, SC, Jun. 1–5, 2008, pp. 48–51.
[40] Z. Peng, X. Yuan, J. Hwang, D. Forehand, and C. Goldsmith, "Superposition model for dielectric charging of RF MEMS capacitive switches under bipolar control-voltage waveforms," *IEEE Trans. Microw. Theory Tech.*, vol. 55, no. 12, pp. 2911–2918, Dec. 2007.
[41] P. Czarnecki, X. Rottenberg, P. Soussan, P. Nolmans, P. Ekkels, P. Muller, H. Tilmans, W. De Raedt, R. Puers, L. Marchand, and I. De Wolf, "New insights into charging in capacitive RF MEMS switches," in *Proc. IEEE Int. Rel. Phys. Symp.*, May 2008, pp. 496–505.
[42] G. Papaioannou, M. Exarchos, V. Theonas, G. Wang, and J. Papapolymerou, "Temperature study of the dielectric polarization effects of capacitive RF MEMS switches," *IEEE Trans. Microw. Theory Tech.*, vol. 53, no. 11, pp. 3467–3473, Nov. 2005.
[43] S. Hofstein, "Proton and sodium transport in SiO_2 films," *IEEE Trans. Electron Devices*, vol. ED-14, no. 11, pp. 749–759, Nov. 1967.

Gaurav Bahl received the B.Eng. degree in electrical engineering from McMaster University, Hamilton, ON, Canada, in 2005, and the M.S. degree in electrical engineering from Stanford University, Stanford, CA, in 2008, where he is currently working toward the Ph.D. degree in the Department of Electrical Engineering, studying dielectric charging in MEMS and drift stability of encapsulated silicon microresonators.

In 2008, he was an Intern at HP Laboratories, Palo Alto, CA, where he published on circumventing charging-related drift issues within the dielectrics of surface electrode actuators.

Mr. Bahl was a 2005 recipient of the Ontario Professional Engineers Foundation for Education Gold Medal.

Renata Melamud received the B.S. degree (with honors) in mechanical engineering from Carnegie Mellon University, Pittsburgh, PA, in 2003, where she was chosen as an Andrew Carnegie Scholar, and the M.S. and Ph.D. degrees in mechanical engineering from Stanford University, Stanford, CA, in 2006 and 2009, respectively. Her dissertation "Temperature Insensitive Micromechanical Resonators" concerned the passive temperature compensation of silicon resonators for frequency references.

She was a Gabilan Stanford Graduate Fellow at Stanford University. She is currently a MEMS Development Engineer at SiTime, Sunnyvale, CA, where she is developing next-generation MEMS resonators for timing references.

Bongsang Kim received the B.S. degree in mechanical design and production engineering from Seoul National University, Seoul, Korea, and the M.S. and Ph.D. degrees in mechanical engineering with an electrical engineering minor from Stanford University, Stanford, CA, in 2004 and 2007, respectively.

From 1998 to 2001, he was a Mechanical Engineer at Hyundai and, in 2005, was an Intern at Agilent Research Laboratories, where he worked on the development of nanosteppers that are capable of $1000g$ acceleration. He is currently working with Prof. Clark Nguyen as a Postdoctoral Researcher at the Berkeley Sensor and Actuator Center (BSAC), University of California, Berkeley. His research interests include RF MEMS, reliability of micro-/nanoscale structures, MEMS packaging, material diffusion, and energy loss and stability of micromechanical resonators.

Dr. Kim was the recipient of the Best Student Award at the 2007 IEEE Frequency Control Symposium and the Best Paper Award at the 2008 BSAC IAB fall meeting.

Saurabh A. Chandorkar received the B.Tech. degree in mechanical engineering from the Indian Institute of Technology, Mumbai, India, in 2003, and the M.S. and Ph.D. degrees in mechanical engineering from Stanford University, Stanford, CA, in 2005 and 2009, respectively. His dissertation entitled "Energy loss mechanisms in micromechanical resonators" focused specifically on the study of thermoelastic dissipation and the Akhieser effect in micromechanical resonators.

He is currently a Postdoctoral Fellow with the Department of Electrical Engineering, Stanford University, where he is working on development of a thermal-actuation-based nanoimprint lithography.

James C. Salvia received the B.S. degree in electrical and computer engineering from Carnegie Mellon University (CMU), Pittsburgh, PA, in 2005, and the M.S. degree in electrical engineering from Stanford University, Stanford, CA, in 2008, where he is currently working toward the Ph.D. degree in electrical engineering.

He was a Research Assistant at CMU, where he developed on-chip magnetic inductors for high-frequency applications. He has also held internships at the Bettis Atomic Power Laboratory, Robert Bosch Corporation, and Atheros Communications, Inc. He is currently with the Stanford Micro Structures and Sensors Laboratory, Stanford University, where his work focuses on circuit development for the stabilization and control of microresonator-based oscillators.

Matthew A. Hopcroft (M'08) received the B.Sc. degree in computer engineering from The George Washington University, Washington, DC, in 1998, the M.Phil. degree from the Department of Engineering, University of Cambridge, Cambridge, U.K., in 2002, and the Ph.D. degree in mechanical engineering from Stanford University, Stanford, CA, in 2007.

He is currently a Research Specialist at the Berkeley Micromechanical Analysis and Design Group and the Berkeley Sensor and Actuator Center, University of California, Berkeley. His research interests include MEMS material property measurements, microscale and portable power systems, and micromechanical resonators.

David Elata (M'01) received the B.Sc. degree in mechanical engineering from the Ben-Gurion University of the Negev, Beersheba, Israel, in 1986, and the M.Sc. and D.Sc. degrees in mechanical engineering from the Technion—Israel Institute of Technology, Haifa, Israel, in 1989 and 1993, respectively.

From 1993 to 1996, he was a Postdoctoral Research Staff Member at the Lawrence Livermore National Laboratory and a Visiting Postdoctoral Fellow in the Department of Geophysics, Stanford University, Stanford, CA. Since 1996, he has been with the Faculty of Mechanical Engineering, Technion. His current research interests are MEMS, solid mechanics, and computational methods. His activity in MEMS includes the modeling and simulation of electrostatic, piezoelectric, and thermoelastic actuation methods and the development of novel design concepts for MEMS devices.

Robert G. Hennessy received the B.S. degree in electrical engineering and computer science from the University of California, Berkeley, in 2005, and the M.S. degree in electrical engineering from Stanford University, Stanford, CA, in 2007, where he is currently working toward the Ph.D. degree in electrical engineering.

His research interests include charge biasing of MEMS and parasitic charging of dielectrics.

Rob N. Candler received the B.S. degree in electrical engineering from Auburn University, Auburn, AL, in 2000, and the M.S. and Ph.D. degrees in electrical engineering from Stanford University, Stanford, CA, as an NDSEG Fellow, in 2002 and 2006, respectively.

He was a Research Engineer from 2006 to 2007 and then a Senior Research Engineer from 2007 to 2008 at the Bosch Research and Technology Center, Palo Alto, CA. During this time, he was also a Consulting Assistant Professor at Stanford University, where he taught a graduate-level course on sensors. Since 2008, he has been with the University of California, Los Angeles, where he is currently an Assistant Professor and the Director of the Sensors and Technology Laboratory and the Nanoelectronics Research Facility.

Roger T. Howe (F'96) received the B.S. degree in physics from Harvey Mudd College, Claremont, CA, and the M.S. and Ph.D. degrees in electrical engineering from the University of California, Berkeley, in 1981 and 1984, respectively.

After faculty positions at Carnegie Mellon University, Pittsburgh, PA, and the Massachusetts Institute of Technology, Cambridge, from 1984 to 1987, he returned to the University of California, where he was a Professor until 2005. He is currently the William E. Ayer Professor in the Department of Electrical Engineering, Stanford University, Stanford, CA. He is a Cofounder of Silicon Clocks, Inc., a start-up company commercializing integrated MEMS resonator-based timing products. His research interests include microelectromechanical system designs, micro- and nanomachining processes, and parallel assembly processes. A focus of his research has been processed to fabricate integrated microsystems, which incorporate both silicon integrated circuits and MEMS. He has made contributions to the design of MEMS accelerometers, gyroscopes, electrostatic actuators, and microresonators.

Dr. Howe served as Cogeneral Chair of the 1990 IEEE MEMS Workshop in Napa, CA, and was the Technical Program Chair of Transducers 2003 in Boston, MA. He is a Subject Editor of the JOURNAL OF MICROELECTROMECHANICAL SYSTEMS. He was the corecipient of the 1998 IEEE Cledo Brunetti Award and was elected to the U.S. National Academy of Engineering in 2005 for his contributions to MEMS processes, devices, and systems.

Thomas W. Kenny received the B.S. degree in physics from the University of Minnesota, Minneapolis, in 1983, and the M.S. and Ph.D. degrees in physics from the University of California, Berkeley, in 1987 and 1989, respectively.

From 1989 to 1993, he was with the NASA Jet Propulsion Laboratory, Pasadena, CA, where his research focused on the development of electron-tunneling high-resolution microsensors. In 1994, he joined the Mechanical Engineering Department, Stanford University, Stanford, CA, where he directs MEMS-based research in a variety of areas, including resonators, wafer-scale packaging, cantilever beam force sensors, microfluidics, and novel fabrication techniques for micromechanical structures. He is the Founder and Chief Technology Officer of Cooligy, Sunnyvale, CA, which is a microfluidics chip cooling components manufacturer, and the Founder and a Board Member of SiTime Corporation, which is a developer of CMOS timing references using MEMS resonators. Since 2006, he has been on leave to serve as Program Manager of the Microsystems Technology Office, Defense Advanced Research Projects Agency, Arlington, VA, starting and managing programs in thermal management (TGP, MACE, NTI, and MCM), nanomanufacturing (TBN), manipulation of Casimir forces (CEE), and the Young Faculty Award. He has authored or coauthored over 200 scientific papers and is the holder of 44 issued patents.

Dr. Kenny is currently the Stanford Bosch Faculty Development Scholar and was the General Chairman of the 2006 Hilton Head Solid State Sensor, Actuator, and Microsystems Workshop.